




ARTICLE

<https://doi.org/10.1038/s41467-019-11147-3>

OPEN

IFN- γ selectively suppresses a subset of TLR4-activated genes and enhancers to potentiate macrophage activation

Kyuho Kang ^{1,2,5}, Mahesh Bachu^{1,5}, Sung Ho Park¹, Keunsoo Kang³, Seyeon Bae¹, Kyung-Hyun Park-Min ¹ & Lionel B. Ivashkiv ^{1,4}

Activation of macrophage proinflammatory and antimicrobial phenotypes is regulated by IFN- γ and LPS via synergistic induction of canonical, inflammatory NF- κ B target genes. However, whether IFN- γ negatively regulates components of the LPS response, and how this may affect macrophage activation, is still unclear. Here we use combined transcriptomic and epigenomic approaches to find that IFN- γ selectively abrogates LPS-induced feedback and alters macrophage metabolic pathways by suppressing TLR4-mediated gene activation. In contrast to superinduction of inflammatory genes via enhancers that bind IRF1 and STAT1, IFN- γ represses target enhancers that bind STAT3. TLR4-activated but IFN- γ -suppressed enhancers comprise two subsets discernable by differential regulation of histone acetylation and recruitment of STAT3, CDK8 and cohesin. Our findings thus show that IFN- γ suppresses feedback inhibitory and metabolic components of TLR responses to enhance macrophage activation; they also provide insights for IFN- γ -mediated selective inhibition of TLR4-induced transcription. Such inhibition can contribute to severe and sustained inflammatory responses.

¹Arthritis and Tissue Degeneration Program and the David Z. Rosensweig Genomics Research Center, Hospital for Special Surgery, New York, NY 10021, USA. ²Department of Biology, Chungbuk National University, Cheongju 28644, Republic of Korea. ³Department of Microbiology, Dankook University, Cheonan 31116, Republic of Korea. ⁴Graduate Program in Immunology and Microbial Pathogenesis, Weill Cornell Graduate School of Medical Sciences, New York, NY 10021, USA. ⁵These authors contributed equally: Kyuho Kang, Mahesh Bachu. Correspondence and requests for materials should be addressed to K.K. (email: kangk@cbnu.ac.kr) or to L.B.I. (email: ivashkiv@hss.edu)

Macrophages are dynamic cells that differentiate into diverse states in response to various stimuli^{1–3}. Macrophages that are activated by inflammatory signals, such as interferon- γ (IFN- γ) and lipopolysaccharide (LPS), termed M(IFN- γ) and M(LPS), respectively, play an important role in host defense against pathogens as well as the pathogenesis of chronic inflammatory diseases^{4–7}. Although IFN- γ via Jak-STAT1 signaling pathway can induce antigen-presentation molecules and chemokines, the expression of inflammatory cytokines (NF- κ B target genes), such as *TNF* and *IL6*, is not activated by IFN- γ alone. In addition, LPS alone transiently activates inflammatory genes but pre-exposure to LPS rather induces tolerance and thereby resistance to subsequent Toll-like receptor (TLR) 4 stimulation. To potentiate activation, IFN- γ primes macrophages and synergizes with LPS to activate inflammatory programs through several molecular mechanisms including chromatin remodeling and metabolic reprogramming at the level of translation^{8–10}.

During TLR4 response, autocrine IFN- β signals through the interferon-stimulated gene factor 3 (ISGF3) complex composed of STAT1/STAT2/IRF9 that binds to interferon-stimulated response elements (ISREs), to induce a feedforward loop in LPS-induced gene expression promoting macrophage activation¹¹. On the other hand, LPS also induces feedback inhibition loops including IL-10-STAT3 anti-inflammatory pathways to prevent excessive inflammation¹². However, the importance of over-riding feedback inhibition by IFN- γ and underlying mechanisms are not well understood. Prolonged exposure to various stimuli fine-tunes the responsiveness of macrophages to secondary stimulation. This feature of innate immune cells, called innate immune memory, plays a key role in various immune responses like endotoxin tolerance during sepsis, trained immunity after vaccination, and inhibition of antimicrobial responses by parasitic infections^{13–16}. Priming of macrophages by IFN- γ exhibits certain similarities to training¹⁰. Most studies of IFN- γ priming have focused on the enhancement of secondary responses to inflammatory challenge, but IFN- γ -mediated attenuation of responses to subsequent stimulation is mostly unexplored.

Epigenomic reprogramming of macrophage-specific enhancers by a variety of micro-environmental stimuli not only contributes to the distinct phenotypes of macrophages in different tissues or diseases states, but also to innate immune memory in macrophages^{17,18}. Signal-dependent transcription factors including NF- κ B, AP-1, and STATs play a critical role in dynamic changes of active enhancer landscapes in macrophages^{19,20}. Our previous work demonstrated that IFN- γ priming mediates genome-wide STAT1 binding with IRF1 at *cis*-regulatory elements to increase histone acetylation to enhance the transcriptional responsiveness to subsequent LPS stimulation⁸. Unbiased transcriptome-wide analysis has revealed that environmental signals not only activate gene expression but also repress distinct gene sets^{21–23}. Molecular mechanisms by which the key macrophage differentiation signals, such as IFN- γ or IL-4 suppress gene expression have been studied using epigenomic approaches. For example, IFN- γ can repress basal anti-inflammatory gene expression programs by two distinct mechanisms: first, IFN- γ induces the deposition of negative histone mark H3K27me3 at promoters through EZH2 recruitment²⁴, and second, IFN- γ deactivates and disassembles enhancers by suppressing binding of MAF and lineage-determining transcription factors²⁵. It has also been reported that IL-4 can antagonize IFN- γ -induced transcriptional responses²⁶, and directly suppress LPS-induced inflammatory responses by STAT6-dependent enhancer deactivation²⁷. Despite these efforts to reveal mechanisms of transcriptional repression by IFN- γ , inhibition of LPS-inducible genes

by IFN- γ at the transcriptomic and epigenomic level has not been elucidated.

In this study, we wish to understand how IFN- γ priming selectively attenuates a component of TLR4-induced genes to strongly activate macrophages by performing a comprehensive transcriptomic and epigenomic analysis using primary human macrophages. We find that LPS-induced genes that are repressed by IFN- γ priming can be subdivided into at least two subsets: those regulated by an IL-10-STAT3 negative feedback loop, and those that function in metabolic pathways and are regulated independently of IL-10. One mechanism of repression involves deactivation of LPS-induced enhancers that are associated with repressed genes. Inhibition of one subset of enhancers that harbors STAT motifs occurs via the suppression of histone acetylation and recruitment of STAT3, CDK8-Mediator, and cohesin. This contrasts with superactivation of TLR4-inducible genes via recruitment of STAT1 to enhancers that harbor IRF motifs. These findings provide insights into mechanisms by which IFN- γ selectively suppresses anti-inflammatory and metabolic components of the TLR response by enhancer deactivation to augment macrophage activation.

Results

Selective inhibition of LPS-induced transcription by IFN- γ . A well-established function of IFN- γ is augmentation of LPS-induced inflammatory gene expression, but little is known about the overall effects of IFN- γ on TLR4-induced transcriptional responses. To examine how IFN- γ alters LPS-induced gene expression, we performed RNA sequencing (RNA-seq) analysis of primary human macrophages cultured with or without IFN- γ for 48 h, followed by a 3 h challenge with LPS (Fig. 1a and Supplementary Fig. 1a, b). We focused on the 3909 differentially expressed genes (FDR < 0.01, > 2-fold differences in expression) in any pairwise comparison among four conditions. *k*-means clustering classified the genes into six gene clusters that were distinctly regulated by IFN- γ and LPS (Fig. 1b, c). Although many of the clusters captured known and previously studied patterns of gene regulation by IFN- γ and/or LPS, there was a large subset of genes (cluster IV, $n = 770$) whose induction by LPS was suppressed by IFN- γ . As the negative regulation of TLR responses by IFN- γ is poorly understood, in this study we focused on class IV genes, and on enhancers that are regulated in a similar manner. As a comparison point and a control, we used class V genes ($n = 541$) that were synergistically induced by IFN- γ and LPS and comprise canonical inflammatory genes such as *IL6*, *IL23A*, and *CXCL9*.

Gene ontology (GO) analysis revealed that each cluster was enriched in genes associated with distinct biological functions (Fig. 1d and Supplementary Data 1). Cluster I, which contains genes basally expressed in human macrophages and repressed by IFN- γ and LPS, was enriched for genes involved in wound healing and related reparative processes; this extends our previous work showing that IFN- γ suppresses basal expression of genes that are inducible by glucocorticoids and IL-4²⁵. In contrast, LPS-inducible genes repressed by IFN- γ (cluster IV) were associated with negative regulation of inflammatory responses, metabolism, and iron transport (Fig. 1d). Closer examination of these genes and comparison to one public dataset (GSE43700²⁸) revealed that cluster IV contains *IL10* and approximately 30% (239/770) of genes in cluster IV correspond to IL-10-inducible genes (Fig. 1e, left, representative genes are shown, and Supplementary Fig. 1c). These results suggest that IFN- γ broadly interrupts the IL-10-mediated LPS-induced negative feedback-loop that negatively regulates inflammation, at least in part by suppressing *IL10* induction. A kinetic experiment showed that IFN- γ suppressed

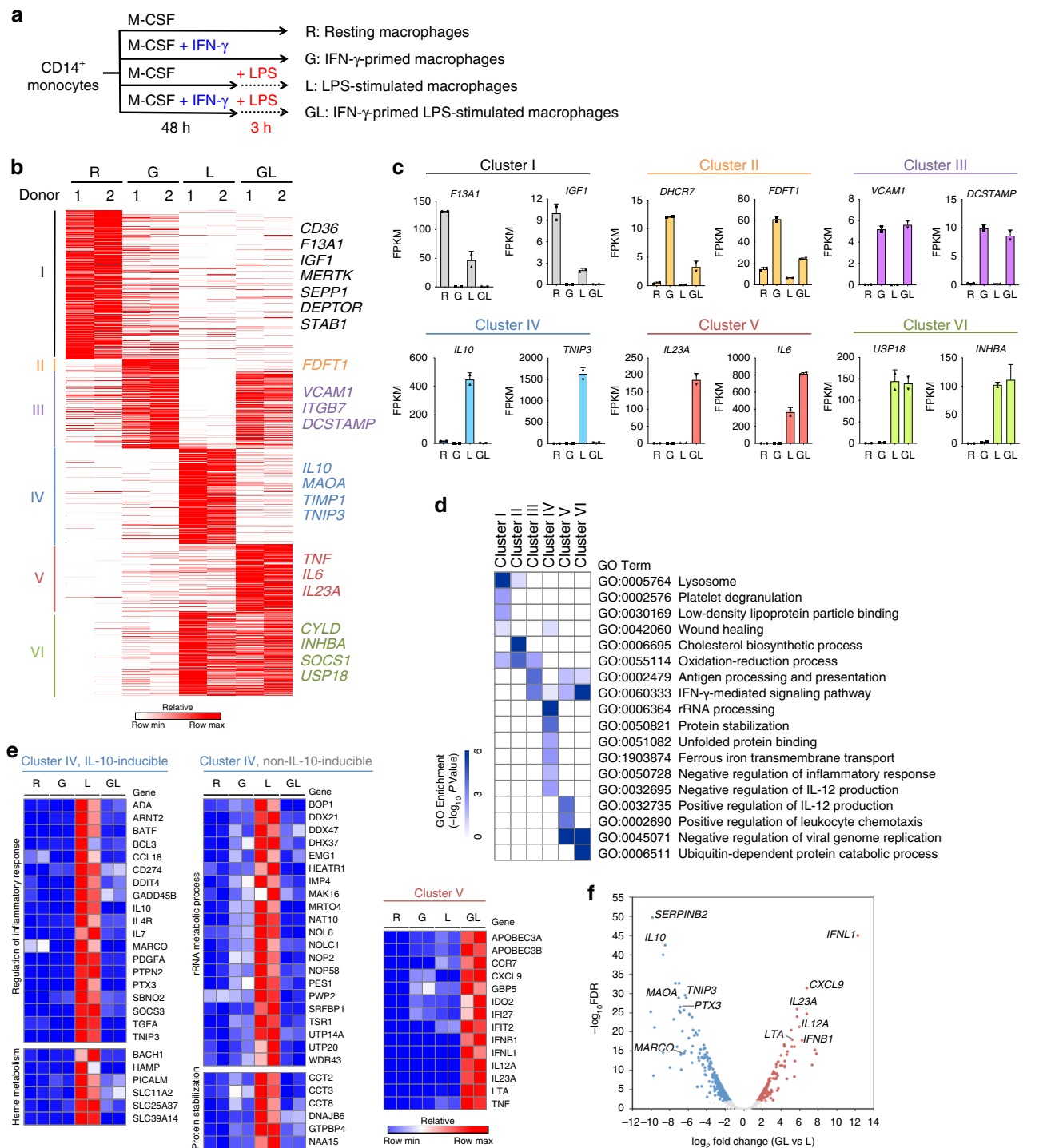


Fig. 1 IFN-γ-mediated reprogramming of TLR4-induced transcriptome in human macrophages. **a** Experimental design: human CD14⁺ monocyte-derived macrophages underwent one of four different combinations of priming for 48 h with IFN-γ before stimulation with LPS (or not) for 3 h: without priming or stimulation (R); primed with IFN-γ without LPS stimulation (G); LPS stimulation only with no priming (L); or primed with IFN-γ and stimulated with LPS (GL). **b** K-means (K = 6) clustering of 3,909 differentially expressed genes in any pairwise comparison among four conditions. Clusters are indicated on the left. **c** Examples of expression of select genes from the six clusters identified in **a**. Each dot in the bar plot represents one donor and error bars represent standard deviation. **d** Heatmap showing the *P*-value significance of GO term enrichment for genes in each cluster. **e** Heatmap showing the relative expression of representative cluster IV genes that are inducible by IL-10 (left), cluster IV genes that are not inducible by IL-10 (middle), and cluster V genes. Distinct biological functions are indicated on the left. IL-10-inducible genes were obtained from GSE43700. **f** Volcano plot of transcriptomic changes between LPS (L) and IFN-γ-primed LPS-stimulated (GL) macrophages; colored dots correspond to genes with significant (FDR < 0.01) and greater than two-fold expression changes. Data from two independent experiments with different donors are depicted

IL10 expression throughout the time course of LPS stimulation (Supplementary Fig. 1d). Interestingly, STAT3 binds to *IL10* locus enhancers and this binding is attenuated by IFN- γ (see below) raising the possibility of a regulatory loop whereby attenuation of STAT3 binding contributes to decreased *IL10* expression, and decreased *IL10* expression results in decreased STAT3 activation. GO and pathway analysis revealed that the IL-10-inducible genes in cluster IV were associated with anti-inflammatory and heme metabolism pathways, whereas the non-IL-10-inducible genes showed enrichment in distinct pathways related to lipid, purine, tryptophan, and iron metabolism; rRNA processing; and protein stabilization and unfolded protein binding (Fig. 1e, middle, representative genes are shown, Supplementary Fig. 1e, f). To test whether IFN- γ affects metabolism by altering the balance between glycolysis and oxidative phosphorylation, we measured extracellular acidification rate (ECAR) as a reflection of glycolysis and oxygen consumption rate (OCR) as a reflection of oxidative phosphorylation. IFN- γ increased ECAR similarly to LPS, and neither stimulus had much effect on OCR (Supplementary Fig. 1g), supporting that IFN- γ contributes to increased glycolysis during macrophage activation.

The two distinct gene subsets in cluster IV could be partially distinguished by induction mediated by Jak-STAT signaling versus mTORC1 signaling and Myc binding at promoters, which is in accord with a previous report⁹ (Supplementary Fig. 1f, h). Cluster IV also includes AP-1-dependent genes such as *MMPs*, which is consistent with previous reports that IFN- γ suppresses AP-1 pathways^{6,29}. In contrast to class IV, class V, which contains genes synergistically induced by IFN- γ and LPS, was enriched in inflammatory cytokine and chemokine genes (Fig. 1c–e). The differential regulation of genes in clusters IV and V by IFN- γ is highlighted in the volcano plot depicted in Fig. 1f. These results identify two groups of LPS-inducible genes that are regulated in opposing directions by IFN- γ and have distinct functions and identify negative regulation of LPS-induced metabolic genes as a new IFN- γ function.

We next tested whether IFN- γ similarly regulated the LPS response in macrophages that were cultured with GM-CSF instead of M-CSF (Supplementary Fig. 2a, b). We found that in GM-CSF-cultured macrophages IFN- γ suppressed LPS-induced *IL10* expression and superinduced *TNF* expression (Supplementary Fig. 2c), similar to M-CSF-cultured macrophages. We then investigated this regulation genome-wide using RNA-seq. Application of the same analysis strategy as we had used with M-CSF-cultured macrophages to GM-CSF-cultured macrophages identified six clusters of genes that we term GM-C1 through GM-C6 (Supplementary Fig. 2d). The patterns of gene expression were similar to those observed with M-CSF-cultured macrophages in Fig. 1b, except the distribution of genes amongst the clusters varied, with a greater proportion of repressed genes (compare cluster I in Fig. 1b to cluster GM-C1 in Supplementary Fig. 2d, e). Notably, cluster GM-C4 recapitulated the regulation observed in cluster IV—attenuation of LPS-induced gene expression by IFN- γ ; furthermore, similarly to cluster IV, cluster GM-C4 contained IL-10 and IL-10-inducible genes (Supplementary Fig. 2c–f). However, there was only a partial overlap between the genes in clusters IV (M-CSF-cultured cells) and GM-C4 (Supplementary Fig. 2g), most likely because GM-CSF promotes a distinct differentiation state and basal gene expression than does M-CSF²².

We wished to test whether initial stimulation with LPS would have a similar effect on the IFN- γ response, namely differential regulation of ISGs resulting in a similar pattern of transcriptome clusters. We stimulated macrophages with LPS using a tolerization protocol and then challenged cells with a 3 h IFN- γ stimulation and performed RNA-seq and clustering analysis

(Supplementary Fig. 3a–h). A similar pattern of gene clusters was observed with this experimental design (Supplementary Fig. 3b) as was observed with the converse experimental design (Fig. 1b), indicating that LPS modulates the macrophage IFN- γ response in a complex manner. Interestingly, we identified a cluster of IFN- γ -inducible genes (termed CL3) whose induction was suppressed by LPS pretreatment (Supplementary Fig. 3b). Cluster CL3 corresponds in gene expression pattern to Cluster IV in Fig. 1b, which contains LPS-inducible genes whose induction was suppressed by IFN- γ pretreatment. GO analysis revealed enrichment in Cluster CL3 of canonical ISGs important in antiviral responses and antigen presentation (Supplementary Fig. 3j). In addition, there were two clusters CL2 and CL5 that were synergistically induced in this experimental system (Supplementary Fig. 3b); CL5 genes were associated with ion homeostasis and chemotaxis, whereas CL2 genes were associated with RNA metabolism (Supplementary Fig. 3j).

IFN- γ inhibits a select subset of LPS-activated enhancers. We wished to understand mechanisms underlying suppression of LPS-inducible genes by IFN- γ and tested the hypothesis that IFN- γ inhibits a subset of LPS-activated enhancers using an epigenomic approach. We defined active enhancers as regions of open chromatin (detected by ATAC-seq) that were located >1 kb away from the TSS, bound lineage-determining transcription factors (TFs) PU.1 and/or C/EBP, and exhibited histone 3 lysine 27 acetylation (H3K27-Ac) in at least one of the four conditions (FDR < 0.05, > 2-fold changes in any pairwise comparison; $n = 20,782$ enhancers, Supplementary Fig. 4b). The enhancer calls were validated relative to DNase-seq and histone 3 monomethylated at lysine 4 (H3K4me1) data for CD14-positive monocytes from ENCODE project (Supplementary Fig. 4c). Similar to the transcriptomic data, enhancers differentially regulated at the H3K27-Ac level sorted into six major clusters (Supplementary Fig. 4a, d and Fig. 2a–c). The patterns of H3K27-Ac regulation in enhancer clusters generally resembled patterns of gene expression in gene clusters. Notably, we detected enhancer clusters whose activation (defined by increased H3K27-Ac) by LPS was either blocked (cluster e4, similar pattern to gene cluster IV) or superinduced (cluster e5, similar pattern to gene cluster V) by IFN- γ (Fig. 2a, b, representative gene tracks shown in Fig. 2c). A similar pattern of regulation was observed at e4 and e5 enhancers for recruitment of the histone acetylase CBP (Supplementary Fig. 4e); these enhancer clusters were not differentiated by overall levels of PU.1 binding (Supplementary Fig. 4f). Thus, IFN- γ also differentially regulates LPS-mediated enhancer activation. We investigated whether similar regulation occurs when IFN- γ and LPS are added to macrophages differentiated for several days with M-CSF, which would have a different enhancer landscape than the recently isolated monocytes that were used in the experiments described above. IFN- γ priming suppressed LPS-induced *IL10* expression, while superinducing *IL6* and *TNF* expression, in M-CSF-differentiated macrophages (Supplementary Fig. 2h, i). Accordingly, IFN- γ also suppressed LPS-induced H3K27-Ac at *IL10* locus enhancers (Supplementary Fig. 2j). Thus, these aspects of IFN- γ -mediated regulation of the LPS response were similar in recently isolated monocytes and M-CSF-differentiated macrophages.

We next tested the relationship between IFN- γ -mediated changes in LPS-induced enhancer and gene activity. Notably, genes associated with enhancer cluster e4 closely correlated with genes in cluster IV, and genes associated with e5 enhancers correlated with cluster V genes (Fig. 2d). These enhancer-associated genes exhibited the expected pattern of gene expression, namely attenuation (e4-associated genes) or superinduction

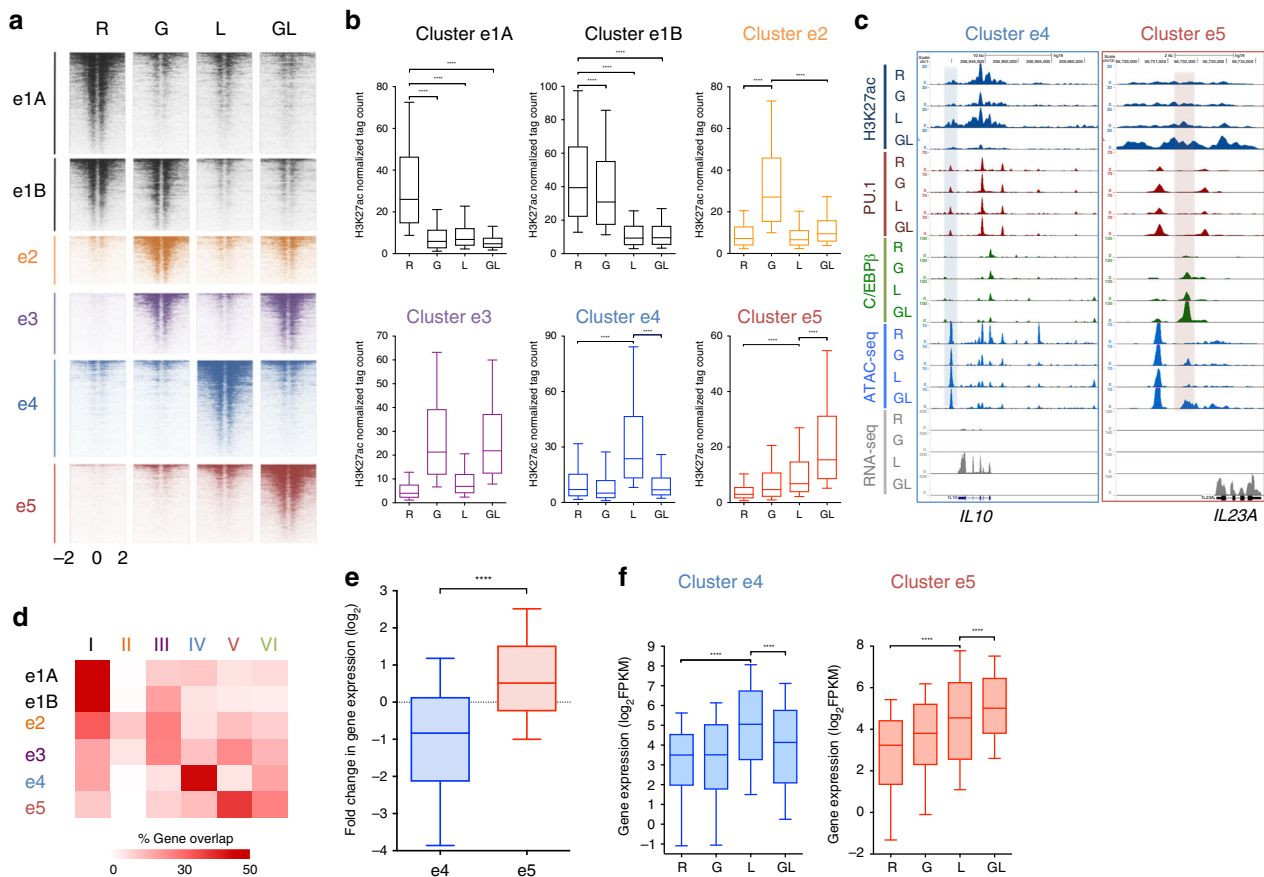


Fig. 2 Selective regulation of LPS-activated enhancer landscapes by IFN- γ . **a** K-means clustering ($K = 5$) of enhancers as shown in Supplementary Fig. 2a further filtered ($FDR < 0.05$, > 2 -fold changes) and subdivided into six enhancer clusters. Heatmaps showing H3K27ac ChIP-seq signals at each enhancer cluster. **b** The boxplots indicate normalized tag counts at each enhancer cluster. **** $p < 0.0001$, paired-samples Wilcoxon signed-rank test. Boxes encompass the twenty-fifth to seventy-fifth percentile changes. Whiskers extend to the tenth and ninetieth percentiles. The central horizontal bar indicates the median. Data are representative of two independent experiments. **c** Representative UCSC Genome Browser tracks displaying normalized tag-density profiles at enhancers of *IL10* and *IL23A* in four conditions. Shaded boxes enclose a cluster e4 enhancer (left) and cluster e5 enhancer (right). **d** Heatmap presentation of the percentage of genes in each cluster (Fig. 1a) that overlap with genes associated with the differentially regulated enhancer clusters identified in panel a. **e** Boxplots showing the change in gene expression between LPS and IFN- γ -primed and LPS-stimulated macrophages for the differentially expressed genes nearest (within 100 kb) to cluster e4 or e5 enhancers. **** $p < 0.0001$ by Welch's t -test. **f** Boxplots showing gene expression in the four indicated conditions for e4- or e5-associated genes. **** $p < 0.0001$ by paired-samples Wilcoxon signed-rank test. Boxes encompass the twenty-fifth to seventy-fifth percentile changes. Whiskers extend to the tenth and ninetieth percentiles. The central horizontal bar indicates the median. Data are representative of two independent experiments

(e5-associated genes) of the LPS response by IFN- γ (Fig. 2e, f). Overall, these findings suggest that IFN- γ selectively modulates LPS-induced enhancer activation to attenuate or boost expression of different subsets of LPS-inducible genes.

TF expression and binding motifs demarcate enhancer clusters.

We reasoned that patterns of TF expression under the four experimental conditions, combined with TF binding motif enrichment in different enhancer clusters, would provide insight into differential regulation of enhancer activity by LPS- and IFN- γ -regulated TFs. IFN- γ and LPS altered the expression of 342 TFs, which were partitioned into the six gene clusters defined in Fig. 1b based on pattern of expression (Fig. 3a, b). Cluster IV TFs (IFN- γ attenuates LPS-induced expression) were distinguished from cluster V TFs (IFN- γ synergizes with LPS) by expression of *STAT3* and AP-1 family members *BATF* and *FOSL2*. A parallel analysis of TF binding motifs enriched under the enhancer peaks defined in Fig. 2b revealed that enhancer clusters e4 and e5 were distinguished by enrichment of AP-1 and STAT motifs in e4 enhancers and IRF motifs in e5 enhancers (Fig. 3c, known motif

analysis, Fig. 3d–e, de novo motif analysis, and Supplementary Figure. 5a, b). The enrichment of AP-1 motifs in e4 enhancers is consistent with inhibition of AP-1 signaling by IFN- γ ^{6,30}. Given that IFN- γ strongly induces and activates *STAT1* (Fig. 3b), which has a predominantly proinflammatory function, the absence of STAT motifs in e5 enhancers may appear puzzling. However, this can be explained by previous work from our laboratory and other groups showing that treatment with IFN- γ for the longer times used in this study results in predominant binding of *STAT1* to IRF sites^{8,20,26,31}, presumably in a complex with IRF proteins; *STAT1* binding measured by ChIP-seq experiments is analyzed below. Known motif analysis (Fig. 3c) suggested binding of *STAT3* to e4 enhancers under LPS-stimulated conditions, which is consistent with the well-established LPS-induced IL-10-*STAT3* autocrine loop, and was further supported by Factorbook ChIP-seq data from ENCODE project showing co-occupancy of *STAT3* with AP-1 at representative cluster e4 enhancers (Fig. 3f). Furthermore, IFN- γ suppressed LPS-induced *STAT3* mRNA expression (Fig. 3b), although *STAT3* protein expression was not changed during the timeframe of these experiments, most likely

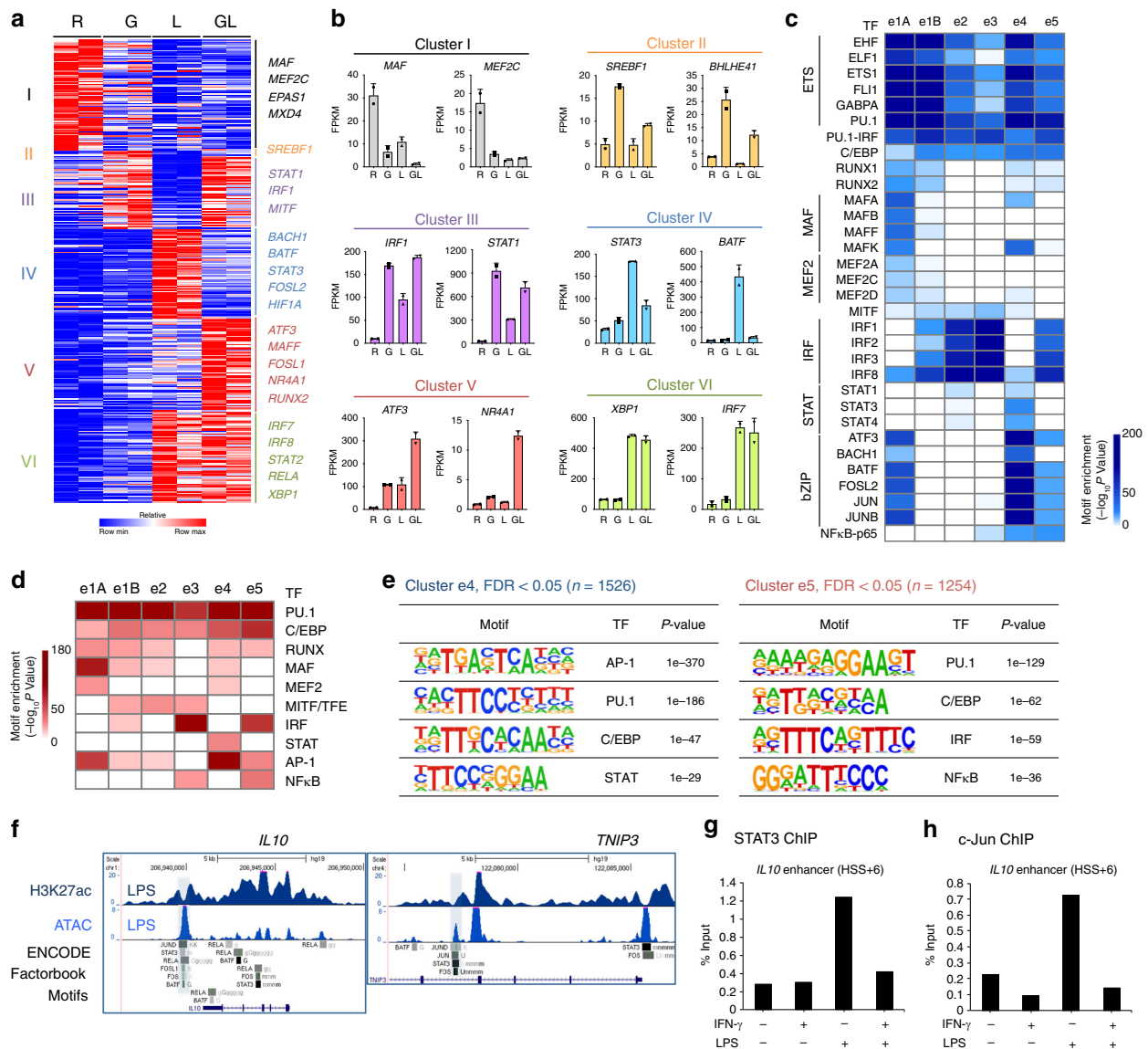


Fig. 3 TF expression and binding motif enrichment in distinct enhancer subsets. **a** Heatmap of gene expression of 91 transcription factors in the clusters defined in Fig. 1a. **b** Examples of TF gene expression from the six identified clusters identified in **a**. **c** Heatmap showing the P -value significance of known motif enrichment in each cluster (defined as in Fig. 2a) and grouped according to TF families (left). **d** Heatmap showing the P -value significance of de novo motif enrichment in six enhancer clusters. **e** The most significantly enriched transcription factor (TF) motifs identified by de novo motif analysis using HOMER in cluster e4 (left) and cluster e5 (right) enhancers. **f** UCSC Genome Browser tracks showing normalized tag density of H3K27ac ChIP-seq and ATAC-seq in LPS-stimulated macrophages. Cumulative TF binding at each e4 enhancer from ENCODE project (Factorbook) is shown below the gene tracks. Boxes enclose representative e4 enhancers at *IL10* (left) and *TNIP3* (right) locus. **g** ChIP-qPCR of STAT3 at the e4 enhancer (HSS + 6) of *IL10*. **h** ChIP-qPCR of c-Jun at the e4 enhancer (HSS + 6) of *IL10*. Data depict experiments with two different donors (**a**) or are representative of two (**b–f**) or three (**g, h**) independent experiments

because of protein stability (Supplementary Fig. 5c). ChIP-qPCR showed that IFN- γ blocked LPS-induced recruitment of STAT3 and the AP-1 protein c-Jun to e4 enhancers at the *IL10* locus (Fig. 3g, h). Overall, these data suggested a role for STAT3 in the regulation of e4 enhancers, and motivated further investigation into how the genomic profile of STAT3 binding is affected by LPS and IFN- γ .

e4 enhancers bind STAT3, which is suppressed by IFN- γ . We next performed STAT3 ChIP-seq experiments and analyzed binding of STAT3 and STAT1 (GSE43036)⁸ to enhancers in clusters e1–e5 after stimulation of human macrophages with LPS, IFN- γ , or both, under the same conditions as used in Fig. 1–3. Interestingly, induction of STAT3 occupancy showed a very

restricted pattern, with a substantial increase only in cluster e4 enhancers in cells stimulated by LPS; this increase in binding was strongly blocked by IFN- γ (Fig. 4a–c; representative gene tracks at *IL10*, *TNIP3*, and *IL4R* loci are shown in Fig. 4d). The much weaker recruitment of STAT3 to e5 enhancers was not affected by IFN- γ , which is consistent with the different regulation of e4 and e5 enhancers. In contrast to STAT3, STAT1 occupancy was increased in most enhancer clusters in cells treated with IFN- γ and was also induced by LPS in clusters e4 and e5 (Fig. 4e–g). As expected^{8,10}, the pattern of STAT1 binding was similar to IRF1 binding (Supplementary Fig. 6b, c). The significance of STAT1 binding to e4 enhancers is not clear, but the increased binding of STAT1 to e5 enhancers in macrophages treated with IFN- γ + LPS is consistent with our previously proposed model of activation of

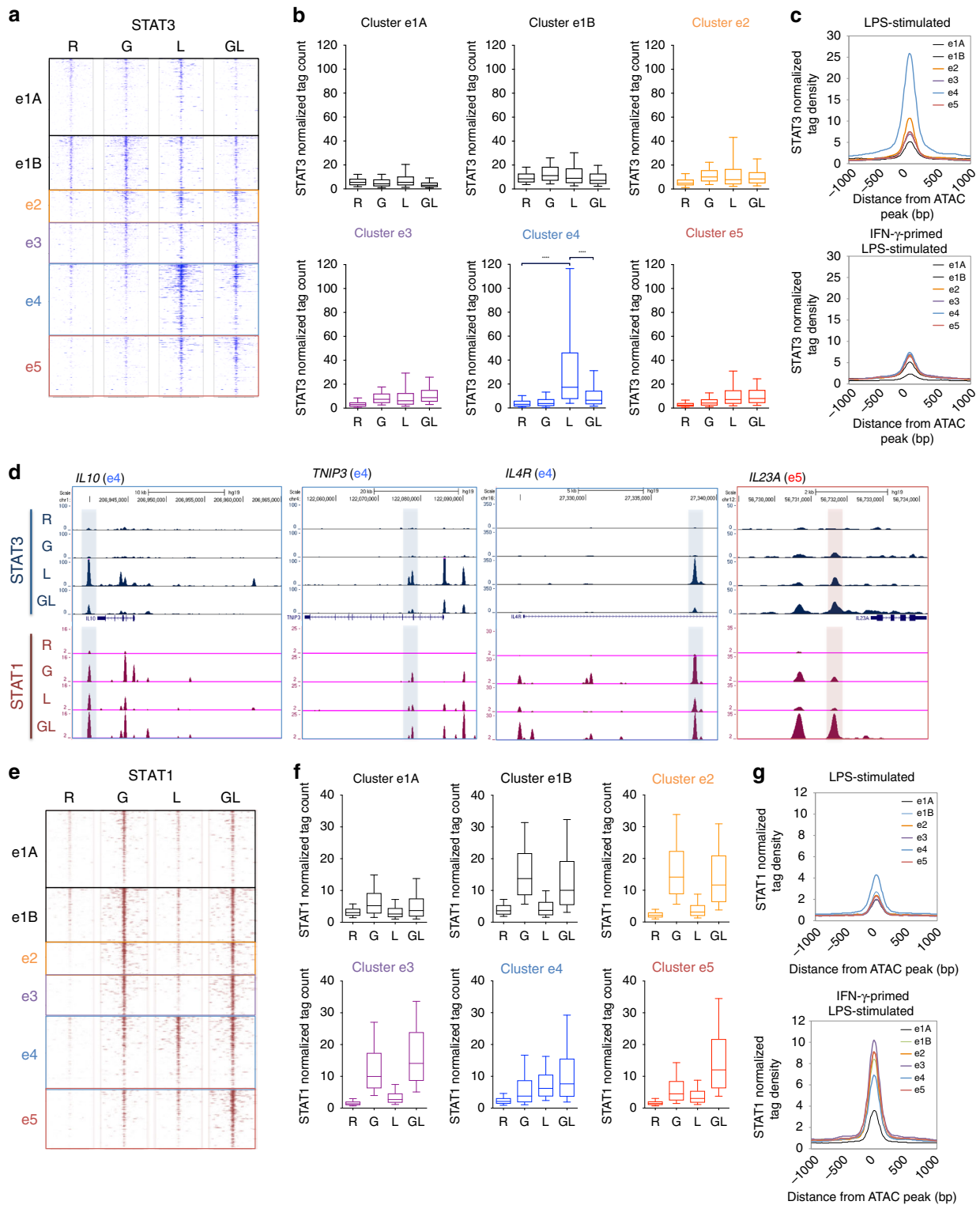


Fig. 4 Differential occupancy of STAT3 and STAT1 at e4 and e5 enhancers. **a** Heatmaps showing STAT3 ChIP-seq signals at each enhancer cluster defined in Fig. 2a. **b** Boxplots depicting normalized tag counts at each enhancer cluster. **** $p < 0.0001$, paired-samples Wilcoxon signed-rank test. **c** Distribution of the average signal of STAT3 ChIP-seq at each enhancer cluster in LPS-stimulated (top) and IFN- γ -primed LPS-stimulated macrophages (bottom). **d** Representative UCSC Genome Browser tracks displaying normalized tag-density profiles at enhancers of *IL10*, *TNIP3*, *IL4R*, and *IL23A* in the four indicated conditions. Boxes enclose cluster e4 enhancer (blue) and cluster e5 enhancer (red). **e** Heatmaps showing STAT1 ChIP-seq signals at each enhancer cluster. **f** The boxplots indicate normalized tag counts at each enhancer cluster. **g** Distribution of the average signal of STAT1 ChIP-seq at each enhancer cluster in LPS-stimulated (top) and IFN- γ -primed LPS-stimulated macrophages (bottom). Data are representative of two independent experiments each of which included at least two independent donors (**a-d**) or are from GSE43036 (**e-g**). Boxes encompass the twenty-fifth to seventy-fifth percentile changes. Whiskers extend to the tenth and ninetieth percentiles. The central horizontal bar indicates the median

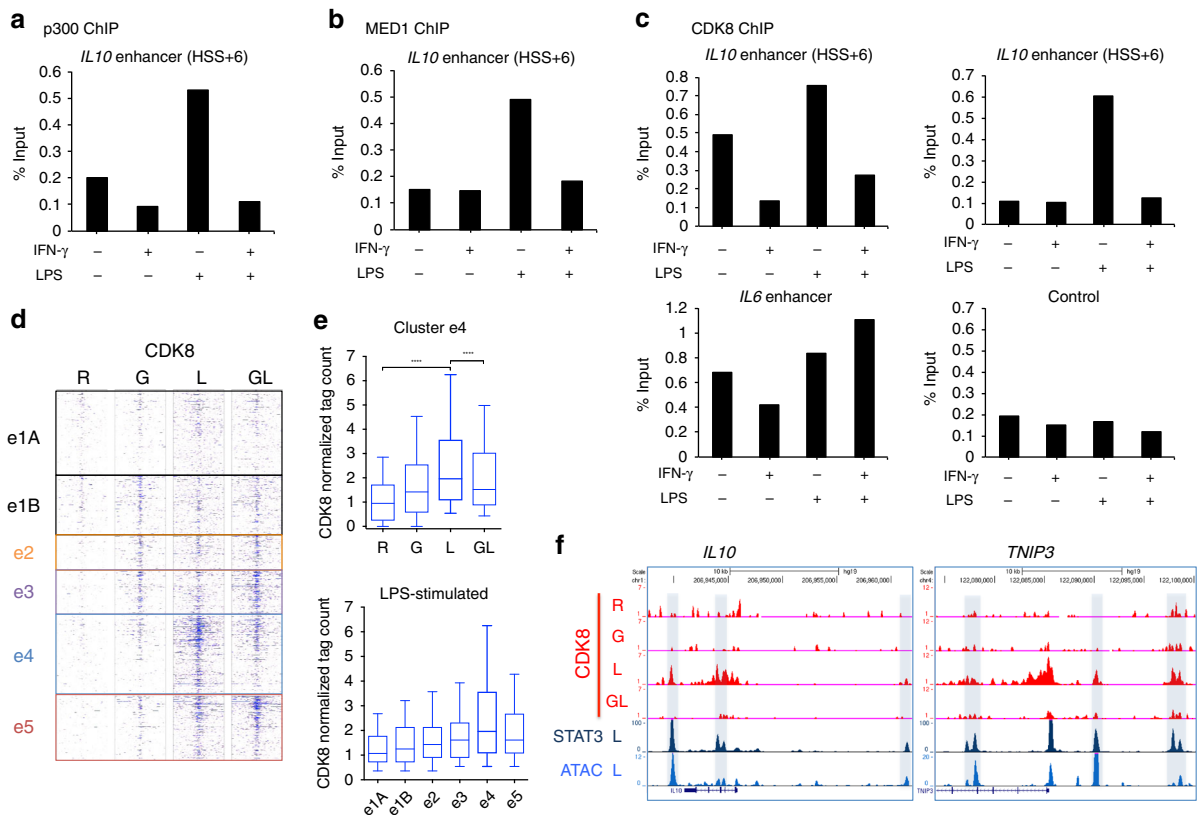


Fig. 5 IFN- γ suppresses coactivator and CDK8 recruitment to e4 enhancers. **a** ChIP-qPCR analysis of p300 occupancy at the e4 enhancer (HSS + 6) of *IL10*. **b** ChIP-qPCR analysis of MED1 occupancy at the e4 enhancer (HSS + 6) of *IL10*. **c** ChIP-qPCR analysis of CDK8 occupancy at e4 enhancers (HSS + 6 and HSS-16) of *IL10* and e5 enhancer of *IL6*. **d** Heatmap showing CDK8 ChIP-seq signals at each enhancer cluster defined in Fig. 2a. **e** The boxplot (top) indicates normalized tag counts at e4 enhancer in the four indicated conditions. **** $p < 0.0001$, paired-samples Wilcoxon signed-rank test. The boxplot (bottom) indicates normalized tag counts at each enhancer cluster in LPS-stimulated macrophages. Boxes encompass the twenty-fifth to seventy-fifth percentile changes. Whiskers extend to the tenth and ninetieth percentiles. The central horizontal bar indicates the median. **f** Representative UCSC Genome Browser tracks displaying normalized tag-density profiles at e4 enhancers of *IL10* and *TNIP3* in the four indicated conditions (CDK8) and the LPS-stimulated condition (STAT3 ChIP-seq and ATAC-seq). Data are representative of three independent experiments (**a–c**), or depict one ChIP experiment using pooled samples from independent experiments using four different donors (**d, e**)

synergy genes by concomitant binding of STAT1 to several enhancers at these gene loci⁸. Overall, the data support a role for IFN- γ -mediated suppression of STAT3 binding at e4 enhancers in the downregulation of expression of associated genes.

IFN- γ suppresses coactivator and CDK8 recruitment. STATs activate gene expression in part by recruiting transcriptional coactivators such as the histone acetyltransferase p300 and Mediator complexes, a subset of which contain the serine kinase CDK8^{32–34}. CDK8 in turn potentiates the transcriptional activity of STAT1 and STAT3 by phosphorylating a serine residue in their transactivation domains. We wished to test the idea that IFN- γ suppresses coactivator recruitment to e4 enhancers (LPS-activated enhancers suppressed by IFN- γ). We first examined coactivator and CDK8 recruitment at the prototypical e4 enhancer associated with the class IV gene *IL10*; as a contrasting control, we used e5 enhancers associated with prototypical class V synergy genes *IL6* and *IL23A*. IFN- γ strongly suppressed LPS-induced recruitment of p300, the MED1 component of Mediator, and CDK8 to *IL10* locus e4 enhancers but not to *IL23A* and *IL6* e5 enhancers (Fig. 5a–c and Supplementary Fig. 7a, b). We followed up these results using ChIP-seq to obtain the genomic profile of CDK8 binding. Strikingly, CDK8 recruitment was most prominent at e4 and e5 enhancers and paralleled their activity (Fig. 5d–f and Supplementary Fig. 7c, d). Namely, LPS-inducible recruitment of CDK8 to e4 enhancers was suppressed by IFN- γ ,

and to e5 enhancers was increased by IFN- γ . Taken together, the data suggest that IFN- γ suppresses recruitment of STAT3 and coactivators to enhancers concomitant with suppressing expression of associated genes.

STAT3 and CDK8 binding define distinct e4 enhancer subsets. As cluster IV genes partitioned into IL-10-dependent and independent genes, we wondered whether e4 enhancers can be similarly subdivided. Closer examination of STAT3 binding to e4 enhancers, when rank-ordered according to tag counts, revealed that e4 enhancers partitioned into two groups, characterized by either high (52%, $n = 787$) or low (48%, $n = 739$) if not absent STAT3 binding (Fig. 6a). We wondered whether STAT3^{hi} peaks corresponded to enhancers that are activated by autocrine IL-10 and began to address this question by performing STAT3 ChIP-seq using macrophages stimulated with recombinant IL-10. Interestingly, STAT3^{hi} e4 enhancers (in cells treated with LPS) corresponded closely to enhancers that bound STAT3 after stimulation with IL-10 (Fig. 6b). To determine which additional features distinguished STAT3^{hi} from STAT3^{lo} e4 enhancers, we performed motif analysis, which revealed selective enrichment of the STAT motif only at STAT3^{hi} e4 enhancers (Fig. 6c). This result coincides with selective enrichment of the STAT motif in promoters of IL-10-inducible cluster IV genes (Supplementary Fig. 1g), which showed higher STAT3 occupancy than promoters of non-IL-10-inducible cluster IV genes (Supplementary Fig. 8a).

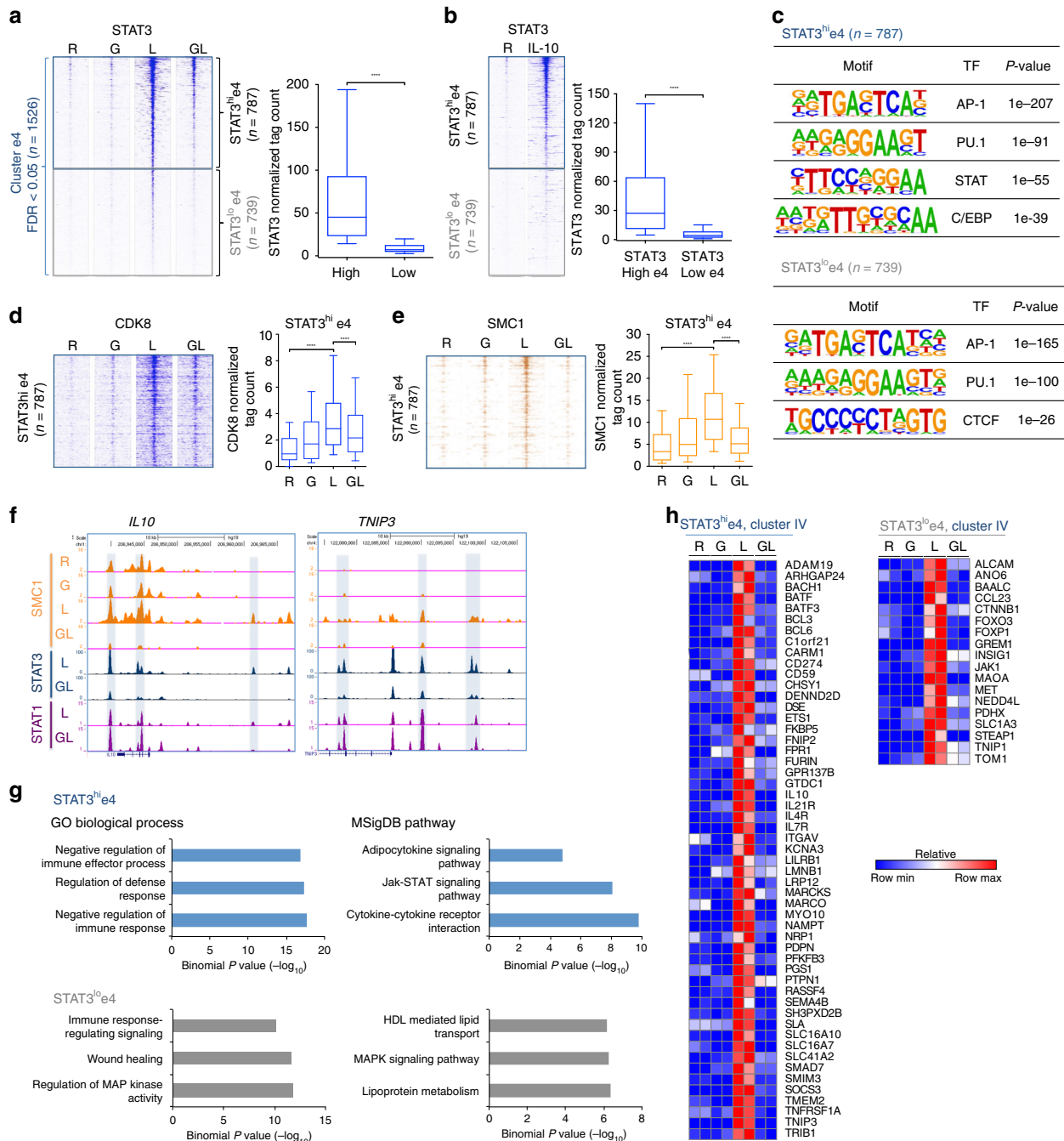


Fig. 6 The strength of STAT3 binding divides e4 enhancers into two subgroups. **a** Heatmaps of STAT3 ChIP-seq signals at cluster e4 enhancers in the four indicated conditions. Enhancers were separated into two subsets: STAT3^{hi}e4 ($n = 787$) and STAT3^{lo}e4 ($n = 739$) based upon a cutoff of \log_2 normalized tag counts = 3. The boxplot (right) depicts normalized tag counts at STAT3^{hi}e4 and STAT3^{lo}e4 enhancers. **b** Heatmaps of STAT3 ChIP-seq signals at two subsets of e4 enhancers (defined in **a**) in resting and IL-10-stimulated macrophages. The boxplot (right) indicates normalized tag counts at STAT3^{hi}e4 and STAT3^{lo}e4 enhancers. **c** The most significantly enriched transcription factor (TF) motifs identified by de novo motif analysis using HOMER at STAT3^{hi}e4 (top) and STAT3^{lo}e4 (bottom) enhancers. **d** Heatmaps of CDK8 ChIP-seq signals at STAT3^{hi}e4 enhancers in the four indicated conditions. The boxplot (right) indicates normalized tag counts at STAT3^{hi}e4 enhancers. **e** Heatmaps of SMC1 ChIP-seq signals at STAT3^{hi}e4 enhancers in the four indicated conditions. The boxplot (right) indicates normalized tag counts at STAT3^{hi}e4 enhancers in four conditions. **** $p < 0.0001$, paired-samples Wilcoxon signed-rank test. **f** Representative UCSC Genome Browser tracks displaying normalized tag-density profiles at e4 enhancers of *IL10* and *TNIP3* in the indicated conditions. **g** Enriched Gene Ontology (GO) and MSigDB pathway categories of genes assigned to STAT3^{hi}e4 enhancers (upper panel) or STAT3^{lo}e4 enhancers (lower panel). **h** Heatmaps of IL-10-inducible cluster IV genes that correspond to STAT3^{hi}e4-associated genes (left panel) or non-IL-10-inducible cluster IV genes that correspond to STAT3^{lo}e4-associated genes (right panel). Data are representative of two independent experiments each of which included at least two independent donors (**a**, **c**, **g**, **h**) or depict one ChIP experiment using pooled samples from independent experiments using two (**b**) or four different donors (**d**, **e**). Boxes encompass the twenty-fifth to seventy-fifth percentile changes. Whiskers extend to the tenth and ninetieth percentiles. The central horizontal bar indicates the median

Furthermore, STAT3^{hi} e4 enhancers showed higher amounts of CDK8 binding compared to STAT3^{lo} e4 enhancers (Fig. 6d). In contrast, CDK8 occupancy was significantly higher at STAT1^{hi} e5 enhancers in IFN- γ -primed LPS-stimulated macrophages (Supplementary Fig. 8b, c). Thus, consistent with the literature, CDK8 occupancy paralleled STAT recruitment during macrophage activation.

CDK8-Mediator complexes and cohesin co-occupy regulatory elements involved in enhancer-promoter looping during gene activation^{35–37}. We thus wished to investigate the relationship between CDK8 and cohesin occupancy in STAT3^{hi} and STAT3^{lo} e4 enhancers. Similar to CDK8 binding, SMC1 occupancy was higher at STAT3^{hi} e4 enhancers, and this binding was induced by LPS and suppressed by IFN- γ (Fig. 6e, f; representative gene tracks at *IL10* and *TNIP3*). We next tested whether the two distinct groups of e4 enhancers (STAT3^{hi} CDK8^{hi} SMC1^{hi} versus STAT3^{lo} CDK8^{lo} SMC1^{lo}) are associated with the different subsets of cluster IV genes, as defined above in Fig. 1. Genomic Regions Enrichment of Annotations Tool (GREAT) analysis of genes associated with STAT3^{hi} e4 enhancers revealed enrichment for IL-10-related GO terms and pathways (Fig. 6g, upper panels and 6h), similar to IL-10-inducible cluster IV genes (Fig. 1e and Supplementary Fig. 1e, f). In contrast, genes associated with STAT3^{lo} e4 enhancers showed distinct functional enrichment for lipid metabolism and MAPK signaling pathways (Fig. 6g, lower panels), which partially resembles pathways associated with non-IL-10-inducible cluster IV genes (Supplementary Fig. 1d–f) and is consistent with enrichment of AP-1 motifs in promoters and enhancers of these genes (Supplementary Fig. 1f, g and 6c). Indeed, genes associated with STAT3^{hi} e4 enhancers were highly represented in the IL-10-inducible cluster IV gene set (53 out of 101; Fig. 6h, left), whereas genes associated with STAT3^{lo} e4 enhancers were included in the non-IL-10-inducible cluster IV gene set (18 out of 36; Fig. 6h, right). In addition, genes associated

with STAT3^{hi} e4 enhancers were more highly induced by IL-10 in monocytes (Supplementary Fig. 8d). Overall, these data suggest that, similar to cluster IV genes, e4 enhancers partition into two groups: those activated by LPS-induced autocrine IL-10 that bind STAT3 as well as CDK8-Mediator and cohesin, and those possibly regulated by AP-1 or other as yet unknown IL-10-independent mechanisms.

IFN- γ functionally suppresses STAT3-bound enhancers. Enhancer activity is associated with recruitment of RNA polymerase II (Pol II) and transcription of enhancer RNAs (eRNAs)^{38–41}. To corroborate the notion that IFN- γ inactivates LPS-induced enhancers, as suggested by the analysis of histone acetylation and CDK8-cohesin recruitment presented above, we more directly measured enhancer activity using ChIP-seq to measure Pol II recruitment. IFN- γ attenuated LPS-induced Pol II recruitment to STAT3^{hi} e4 enhancers (Fig. 7a, b; representative gene tracks at *IL10* locus; HSS + 6 and HSS -16 mark enhancers). In contrast, IFN- γ increased Pol II recruitment to STAT1^{hi} e5 enhancers (Supplementary Fig. 9a, b; representative gene tracks at *IL23A* locus). eRNA could not be reliably measured genome-wide by RNA-seq, but IFN- γ -mediated suppression was clearly seen at enhancers of select genes such as *IL10* (Fig. 7b, gene tracks 5–8) and was confirmed by qPCR (Fig. 7c and Supplementary Fig. 9c, d). Locked nucleic acid-mediated knockdown of *IL10* eRNA at enhancers located 16 kb upstream (HSS-16) or 6 kb downstream (HSS + 6) of the *IL10* TSS suppressed *IL10* mRNA expression (Fig. 7d), supporting a functional role for eRNA and for IFN- γ -regulated enhancer activity.

Discussion

Investigation of IFN- γ transcriptional responses has primarily focused on gene activation during M(IFN- γ) macrophage differentiation, which is linked to the IFN- γ signature observed in

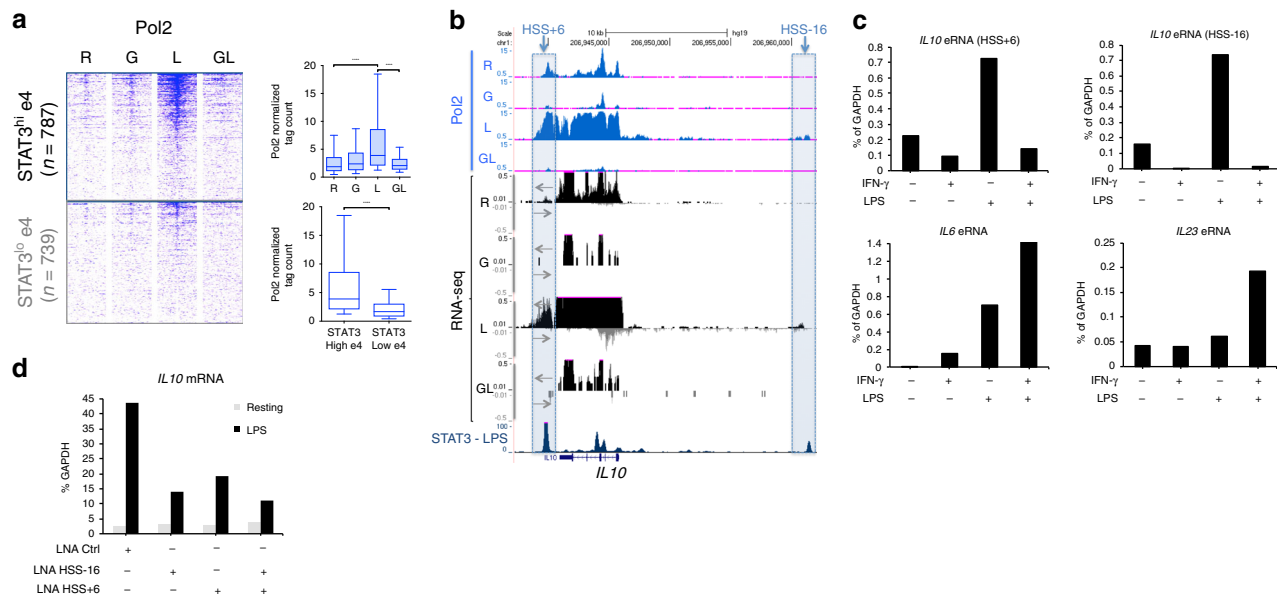


Fig. 7 IFN- γ -mediated functional deactivation of STAT3-bound e4 enhancers. **a** Heatmaps of Pol II ChIP-seq signals at STAT3^{hi}e4 and STAT3^{lo}e4 enhancers (defined in Fig. 6a). The boxplots indicate normalized tag counts at STAT3^{hi}e4 enhancers in the four indicated conditions (top) and at STAT3^{hi}e4 and STAT3^{lo}e4 enhancers in LPS-stimulated macrophages (bottom). **** $p < 0.0001$, paired-samples Wilcoxon signed-rank test. Boxes encompass the twenty-fifth to seventy-fifth percentile changes. Whiskers extend to the tenth and ninetyth percentiles. The central horizontal bar indicates the median. **b** Representative Genome Browser tracks showing RNA polymerase II (Pol II) occupancy, strand-specific RNA transcripts, and STAT3 occupancy (LPS condition) at enhancers of *IL10*. Boxes enclose HSS + 6 (left) and HSS-16 (right). **c** RT-qPCR analysis of enhancer RNA (eRNA) expression at two e4 enhancers (top, *IL10*-HSS + 6 and *IL10*-HSS-16) and two e5 enhancers (bottom, *IL6* and *IL23A*). Data are representative of three independent experiments. **d** RT-qPCR analysis of *IL10* mRNA in resting and LPS-stimulated macrophages transfected with the indicated LNAs (*IL10*-HSS-16 eRNA and *IL10*-HSS + 6 eRNA). Data are representative of two independent experiments

autoimmune diseases, and on synergistic activation of inflammatory genes in cooperation with inflammatory factors such as TLR ligands^{7,10,42,43}. However, negative regulation of TLR-induced gene expression, and its potential functional consequences and underlying mechanisms are not well understood. This study used combined transcriptomic and epigenomic approaches to obtain several new insights into negative regulation of TLR-induced gene expression by IFN- γ . First, IFN- γ selectively represses induction of IL-10-inducible anti-inflammatory genes and also distinctly regulates a subset of metabolic genes. Suppression of IL-10-mediated feedback serves to amplify inflammatory gene activation, whereas suppression of metabolic genes, for example genes involved in fatty acid metabolism linked to M (IL-4) activation, may promote M(IFN- γ + LPS) differentiation. Second, IFN- γ inhibits TLR4-induced genes by targeting associated TLR4-activated enhancers to suppress histone acetylation. Third, IFN- γ inhibits at least two distinct subsets of enhancers, one of which is characterized by enrichment of STAT binding motifs and TLR-induced recruitment of STAT3, CDK8, and cohesin. A distinct suppressed enhancer subset is enriched for AP-1 motifs and may regulate metabolic genes. Fourth, suppressed enhancers differ from enhancers associated with super-activated synergy genes as the latter harbor IRF instead of STAT motifs and bind STAT1 instead of STAT3. However, TLR-inducible enhancers that are modulated by IFN- γ share the property of CDK8 occupancy, suggestive of binding by a select CDK8-containing Mediator complex. Our findings provide insights into previously unexplored mechanisms that selectively regulate TLR responses to promote inflammatory gene activation and M(IFN- γ + LPS) macrophage differentiation.

IFN- γ represses basal gene expression in resting macrophages by two distinct epigenetic mechanisms: (1) induction of the negative histone mark H3K27me3 by recruiting EZH2 to promoters²⁴ (2) suppression of the active enhancer histone mark H3K27ac by inhibiting key enhancer-occupying transcription factors, such as MAZ²⁵. Only a small number of genes is regulated by IFN- γ -mediated direct deposition of H3K27me3, and we did not detect this inhibitory mechanism in the suppression of LPS-induced gene expression. Other groups have suggested that the transcription factors induced by different stimuli, such as IL-4-STAT6²⁷ and nuclear receptors (PPARs and LXRs) can directly suppress gene transcription⁴⁴. However, our data did not support a direct repressive role for IFN- γ -induced STAT1 binding at LPS-activated *cis*-regulatory elements, such as promoters and enhancers. Although we cannot rule out the possibility of STAT1 functioning as a transcriptional repressor, it is more likely that IFN- γ mainly mediates the suppression of gene expression by more indirect mechanisms such as STAT1-induced expression of inhibitors of signaling or transcription. In line with this notion, we have found that a full priming effect requires greater than 3 h of IFN- γ stimulation⁸. It is likely that the patterns of gene expression will vary depending on the relative timing of IFN- γ and LPS stimulation. Future work is needed to investigate the effects of timing to address whether IFN- γ -induced STAT1 has any direct repressive functions in other systems.

In macrophages, it has been shown that IL-10, via STAT3, plays a pivotal role in the induction of anti-inflammatory factors, such as *BCL3*, *IL4R*, and *TNIP3*⁴⁵, and in regulating an mTORC1-mediated metabolic program including *DDIT4*⁴⁶. Thus, inactivation of the LPS-induced IL-10-STAT3-negative regulatory pathway by IFN- γ can contribute to uncontrolled chronic inflammatory responses. Our epigenomic analysis has identified previously uncharacterized LPS-activated enhancer regions (cluster e4), which are selectively inhibited by IFN- γ . Notably, IFN- γ suppressed LPS-inducible STAT3 binding at e4 enhancers that showed loss of active enhancer marks including

histone acetylation, CDK8-cohesin occupancy, and eRNA-related RNA polymerase II. The e4 enhancers with strong recruitment of STAT3 (STAT3^{hi} e4) showed substantial overlap with enhancers that bind STAT3 as part of the canonical IL-10-induced anti-inflammatory program; a similar overlap was observed between e4-associated and IL-10-inducible genes. Given that LPS-inducible STAT3 binding is related to IL-10-induced anti-inflammatory programs, our findings may provide additional insight into the paradoxical effect of Jak inhibitors on the LPS response, namely that they inhibit STAT3-mediated feedback inhibition⁴⁷. A distinct subset of e4 enhancers with low or minimal STAT3 binding after LPS stimulation (STAT3^{lo} e4) was associated with a distinct IL-10-independent gene set with different functions, such as MAPK signaling pathway and lipid metabolism. We gained new insights into how IFN- γ negatively regulates the expression of LPS-induced autocrine IL-10, which is a major direct inducer of STAT3 activation in response to LPS. Previous work has shown that IFN- γ inhibits TLR-induced autocrine IL-10 production by suppressing AP-1-related pathway, which is related to the differential regulation of MAPK and GSK3 activity⁴⁸. The current study extends this work to suggest that negative regulation of signaling leads to suppression of LPS-induced *IL10* expression via epigenetic deactivation of enhancers at the *IL10* locus.

In addition to inhibition of LPS-induced IL-10-STAT3 autocrine feedback loop, IFN- γ suppressed induction of other components of the LPS response that are independent of IL-10. In line with previous work⁹, IFN- γ inhibited transcription of genes that are involved in the ribosomal RNA processing and protein stabilization and downstream of mTORC1 signaling and Myc. A recent study utilizing co-stimulation of mouse macrophages with IFN- γ and IL-4 suggested that Myc is associated with a component of the IL-4 response that is resistant to suppression by IFN- γ ²⁶. Our findings suggest that prolonged exposure to IFN- γ that suppresses Myc may overcome resistance of IL-4 genes to IFN- γ . mTORC1 and Myc are major regulators of cellular metabolism, and IFN- γ repressed genes are involved in various metabolic processes, such as iron transport, purine synthesis, tryptophan metabolism, and lipid metabolism. Of these, lipid metabolism is implicated in M(IL-4) function, tryptophan metabolites in anti-inflammatory responses, and iron transport in host defense. Future work will be needed to determine how regulation of these IL-10-independent TLR4-induced metabolic pathways by IFN- γ contributes to the M(IFN- γ + LPS) phenotype^{49–51}. Overall, IFN- γ -mediated inhibition of anti-inflammatory, translational, and metabolic components of the LPS response is likely coordinated to enable a fully classically activated macrophage phenotype.

Our findings highlight differences in function and mode of regulatory element binding between STAT1 and STAT3 during macrophage activation and LPS challenge. Previous work has shown that during IFN- γ -mediated priming of macrophages, the genomic profile of STAT1 binding changes from STAT sites to IRF sites, which STAT1 can occupy as part of complexes with IRF1 or (after LPS stimulation) as part of the ISGF3 complex^{8,20}. In line with these reports, we found that STAT1 binds to IRF sites coordinately with IRF1 in e5 enhancers and that joint stimulation with IFN- γ + LPS increased STAT1 binding, which correlated with increased enhancer activity (as assessed by histone acetylation) and superinduction of associated cluster V genes. In contrast, STAT3 bound to e4 enhancers that are enriched for STAT motifs, and joint stimulation with IFN- γ + LPS decreased STAT3 binding, which correlated with decreased enhancer activity and suppression of associated cluster IV genes. These results support a model whereby intrinsic DNA sequences (TF binding motifs) in genomic regulatory elements determine whether IFN- γ primes or suppresses activation of an enhancer by LPS. Namely, in

IFN- γ -primed macrophages enhancers that contain IRF but not STAT sites (e.g., e5 enhancers) are subject to regulation mostly by STAT1 and exhibit enhanced LPS responses, whereas enhancers that also contain a STAT site are regulated by STAT3 and exhibit attenuated LPS responses. Motif analysis also found that AP-1 motif was highly enriched at STAT3-bound enhancers, which are suppressed by IFN- γ , suggesting that IFN- γ -regulated AP-1 transcription factors including BATF and FOSL2 might serve as auxiliary transcription factors and cooperate with STAT3 to regulate e4 enhancers. Identifying additional auxiliary transcription factors that cooperate with STAT1 and STAT3 to drive expression of different LPS-regulated gene sets may provide further insight into STATs-dependent transcriptional regulation in a gene-specific manner.

In summary, this study provides insights about how two stimuli can cooperate at the epigenomic level to achieve differential regulation of gene sets with distinct and even opposing functions. In the case of IFN- γ and LPS, differential regulation of enhancers with different sequence architecture results in decreased expression of anti-inflammatory and metabolic genes, with super-induction of inflammatory genes that may enhance inflammatory responses. The distinct enhancer classes can potentially be targeted to restrain excessive inflammation.

Methods

Cell culture. Peripheral blood mononuclear cells were obtained from blood leukocyte preparations purchased from the New York Blood Center by density gradient centrifugation with Ficoll (Thermo Fisher Scientific) using a protocol approved by the Hospital for Special Surgery Institutional Review Board. The samples were anonymous and the investigators do not have access to any identifiable private information. As per the guidelines on Human Subjects Research in the PHS SF424 (R&R) Application Guide and underlying documentation, work with purchased de-identified blood products does not constitute human subjects research; informed consent was not obtained at Hospital for Special Surgery. Primary human CD14⁺ monocytes were obtained from peripheral blood, using anti-CD14 magnetic beads, as recommended by the manufacturer (Miltenyi Biotec). Monocytes were cultured in RPMI 1640 medium (Invitrogen) supplemented with 10% heat-inactivated defined FBS (HyClone Fisher), penicillin/streptomycin (Invitrogen), L-glutamine (Invitrogen), and 10 ng/ml human macrophage colony-stimulating factor (M-CSF; Peprotech) or 20 ng/ml of granulocyte macrophage colony-stimulating factor (GM-CSF) in the presence or absence of 100 U/ml human IFN- γ (Roche) as indicated; IFN- γ was added at the same time as M-CSF or GM-CSF at initiation of cultures. LPS was purchased from Invivogen (tlrl-3pelps). The order of addition of IFN- γ and LPS were reversed in LPS priming experiments (Supplementary Fig. 3) with LPS priming was followed by IFN- γ stimulation for 3 h. CD14⁺ monocytes were also allowed to differentiate for 7 days in M-CSF (20 ng/ml) with intermittent addition of M-CSF (20 ng/ml) every 2 days (Supplementary Fig. 2h-j). IFN- γ priming in these prolonged macrophage differentiation cultures was done on days 6 and 7 for 48 h.

Analysis of RNA. Total RNA was extracted from cells using RNeasy Mini kit (QIAGEN), and 500 ng of total RNA was reverse transcribed using the RevertAid First Strand cDNA Synthesis kit (Fermentas). Real-time PCR was performed in triplicate with Fast SYBR Green Master Mix and 7500 Fast Real-time PCR system (Applied Biosystems). Primer sequences are provided in the Supplementary Table 1.

RNA-seq. After RNA extraction, libraries for sequencing were prepared using the Illumina TruSeq RNA Library Prep Kit following the manufacturer's instructions. High-throughput sequencing (50 bp, paired-end) was performed at the Genomics Resources Core Facility of Weill Cornell Medicine. On average 100 million reads were obtained per sample. Sequenced reads were mapped to reference human genome (hg19 assembly) using STAR aligner⁵² with default parameters, and Cufflinks version 2.2.1⁵³ was used to estimate the abundance of transcripts. The expression levels of genes in each sample were normalized by means of fragments per kilobase of transcript per million mapped reads (FPKM). The concordance between replicates was very high (R^2 range, 0.943–0.964).

RNA-seq analysis. Differentially expressed genes (DEGs) were identified using edgeR v3.16.5^{54,55}. Read counts for edgeR analysis were obtained with featureCounts v1.5.1⁵⁶. After eliminating absent features (zero counts), the raw counts were normalized with edgeR, followed by differential expression analysis. Significantly up or downregulated genes were defined as expressed genes with p -value adjusted for multiple testing (FDR) < 0.01 and \log_2 fold-change of at least 1. To

generate the heatmap of K-mean clusters, we used GENE-E (Broad Institute) set to global comparison and average-centered. The value of K was chosen at 6 because lower values failed to identify all meaningful clusters and higher values subdivided meaningful clusters. To find the GO terms enriched in differentially regulated genes, we used the DAVID web-tool⁵⁷, Cluster Profiler, and Gene Set Enrichment Analysis (GSEA) of MSigDB gene sets (Hallmark, KEGG, and REACTOME).

Gene expression analysis of IL-10 stimulated human monocytes. Microarray data sets were retrieved from GSE43700. The raw data were normalized by a quantile normalization method using the preprocessCore package in R. Normalized expression levels were averaged within the same condition and fold-change of the average for each gene was calculated.

Western Blotting. Whole-cell extracts from CD⁺ 14 monocytes for various treatment conditions were prepared in KalB lysis buffer (150 mM NaCl, 50 mM Tris-HCl (pH 7.5), 1% (v/v) Triton X-100, 1 mM EDTA, 1xPhosSTOP EASYPACK, Pefabloc and complete EDTA-free Protease inhibitor cocktail), fractionated by SDS-PAGE and transferred to a polyvinylidene difluoride membrane as per the manufacturer's protocols (Bio-Rad). Proteins of interest were probed with antibodies against STAT3 (1:1000, Cell Signaling Technologies, Cat. No: 12640), phospho-p38(1:1000, Cell Signaling Technologies, Cat. No: 9215), and p38 (1:1000, Cell Signaling Technologies, Cat. No: 9212) at 4 °C for overnight followed by detection using HRP-conjugated sheep anti-rabbit IgG antibody and visualized with the Pierce ECL western blotting substrate (Thermo Scientific) as per the manufacturer protocol. Original images of the blots are provided in Source Data file.

Seahorse metabolic analysis. The real-time extracellular acidification rate (ECAR) and oxygen consumption rate (OCR) were measured using the XF96 extracellular flux analyzer (Seahorse Bioscience, North Billerica, MA, USA) with the Glycolysis Stress Kit (Seahorse Bioscience) following the manufacturer's instructions. The measurement was normalized to relative level of DNA determined by measuring the fluorescence intensity of cells stained by SYTO 24 green fluorescent nucleic acid stain (Molecular Probes, Eugene, OR). Briefly, human CD14⁺ monocytes were seeded on a pretreated poly-L-lysine-coated XF96 cell culture microplates (Seahorse Bioscience) at a seeding density of 1.6×10^5 cells per well and treated with IFN- γ (100 U/ml) for 2 days and then stimulated with LPS (50 ng/ml). Before assay, cells were rinsed twice and kept in pre-warmed XF assay medium (pH 7.4) supplemented with 1 mM glutamine in a 37 °C non-CO₂ incubator for an hour, and then the rate was measured at 37 °C in 7–8 replicates (separate wells) by using the following compounds in succession: 10 mM glucose, 1 μ M oligomycin, and 50 mM 2-DG. Basal OCR was measured before drug exposure. We calculated the glycolytic function metrics as directed in the glycolysis stress kit manual (Seahorse Bioscience). The ECAR and OCR measurements from four independent donors are provided in Source Data file.

ChIP and ChIP-seq. Cells were crosslinked for 5 min at room temperature by the addition of one-tenth of the volume of 11% formaldehyde solution (11% formaldehyde, 50 mM HEPES pH 7.5, 100 mM NaCl, 1 mM EDTA pH 8.0, 0.5 mM EGTA pH 8.0) to the growth media followed by 5 min quenching with 100 mM glycine. Cells were pelleted at 4 °C and washed with ice-cold PBS. The crosslinked cells were lysed with lysis buffer (50 mM HEPES-KOH pH 7.5, 140 mM NaCl, 1 mM EDTA, 10% glycerol, 0.5% NP-40, and 0.25% Triton X-100) with protease inhibitors on ice for 10 min and washed with washing buffer (10 mM Tris-HCl, pH 8.0, 200 mM NaCl, 1 mM EDTA, 0.5 mM EGTA) for 10 min. The lysis samples were resuspended and sonicated in sonication buffer (10 mM Tris-HCl, pH 8.0, 100 mM NaCl, 1 mM EDTA, 0.5 mM EGTA, 0.1% Na-Deoxycholate, 0.5% N-lauroylsarcosine) using a Bioruptor (Diagenode) with 30 s ON, 30 s OFF on high power output for 18 cycles. After sonication, samples were centrifuged at 14,000 rpm for 10 min at 4 °C and 5% of sonicated cell extracts were saved as input. The resulting whole-cell extract was incubated with Protein A Agarose for ChIP (EMD Millipore) for 1 h at 4 °C. Pre-cleared extracts were then incubated with 50 μ l (50% v/v) of Protein A Agarose for ChIP (EMD Millipore) with 5 μ g of the appropriate antibody overnight at 4 °C. ChIP lysates were generated from 2×10^7 to 3×10^7 cells (for PU.1, C/EBP β , STAT3, c-Jun, and RNA Polymerase II ChIP) or 10×10^7 cells (for p300, MED1, CDK8, and SMC1 ChIP) respectively. ChIP antibodies against PU.1 (sc-352), C/EBP β (sc-150), STAT3 (sc-482), c-Jun (sc-1694), p300 (sc-585) and CDK8 (sc-1521) were from Santa Cruz Biotechnology. Antibodies against RNA Polymerase II (MMS-126R) were from Covance. Antibodies against MED1 (A300–793A) and SMC1 (A300–055A) were from Bethyl Laboratories. After overnight incubation, beads were washed twice with sonication buffer, once with sonication buffer with 500 mM NaCl, once with LiCl wash buffer (10 mM Tris-HCl pH 8.0, 1 mM EDTA, 250 mM LiCl, 1% NP-40), and once with TE with 50 mM NaCl. DNA was eluted in freshly prepared elution buffer (1% SDS, 0.1 M NaHCO₃). Cross-links were reversed by overnight incubation at 65 °C. RNA and protein were digested using RNase A and Proteinase K, respectively and DNA was purified with ChIP DNA Clean & Concentrator™ (Zymo Research). For ChIP-qPCR assays, immunoprecipitated DNA was analyzed by quantitative real-time PCR and normalized relative to input DNA amount.

For ChIP-seq experiments, 10 ng of purified ChIP DNA per sample were ligated with adaptors and 100–300 bp DNA fragments were purified to prepare DNA libraries using Illumina TruSeq ChIP Library Prep Kit following the manufacturer's instructions. ChIP libraries were sequenced (50 bp single end reads) using an Illumina HiSeq 2500 Sequencer at the Epigenomic Core Facility of Weill Cornell Medicine per manufacturer's recommended protocol. Because of limitations on cell numbers and to decrease variability related to differences among individual donors, chromatin immunoprecipitations were performed using pooled samples from more than two (for STAT3) or four (for CDK8 and SMC1) different donors. For STAT3, a second experiment with pooled samples from several donors was performed and congruence between the replicates was assessed by generating scatter plots and estimating Pearson correlation coefficients (Fig. S4A). After ascertaining close correlation between replicates, we performed bioinformatic analysis using replicate 1 and confirmed key results using replicate 2. The H3K27ac, STAT1 and IRF1 data were from GSE43036.

ATAC-seq. ATAC-seq was performed as described⁵⁸. Fifty thousand cells were centrifuged at 500 × g for 5 min at 4 °C. Cell pellets were washed once with 1x PBS and cells were pelleted by centrifugation using the previous settings. Cell pellets were resuspended in 25 µl of lysis buffer (10 mM Tris-HCl pH 7.4, 10 mM NaCl, 3 mM MgCl₂, 0.1% IGEPAL CA-630) and centrifuged immediately 500 × g for 10 min at 4 °C. The cell pellet was resuspended in the transposase reaction mix (25 µL 2 × TD buffer (Nextera DNA Sample Preparation Kit), 2.5 µL Illumina Tn5 transposase and 22.5 µL nuclease-free water). The transposition reaction was carried out for 30 min at 37 °C. Directly following transposition, the sample was purified using a QIAGEN MinElute Purification Kit. Then, we amplified library fragments using NEBNext 2x PCR master mix and 1.25 M of Nextera PCR primers, using the following PCR conditions: 72 °C for 5 min; 98 °C for 30 s; and thermocycling at 98 °C for 10 s, 63 °C for 30 s, and 72 °C for 1 min. The libraries were purified using a QIAGEN PCR purification kit yielding a final library concentration of ~30 nM in 20 µL. Libraries were amplified for a total of 10–13 cycles and were subjected to high-throughput sequencing using the Illumina HiSeq 2500 Sequencer.

ChIP-seq and ATAC-seq analysis. For ChIP-seq and ATAC-seq experiments, sequenced reads were aligned to reference human genome (GRCh37/hg19 assembly) using Bowtie2 version 2.2.6 (Langmead and Salzberg, 2012) with default parameters, and clonal reads were removed from further analysis. A minimum of 20 million uniquely mapped reads were obtained for each condition. We used the makeTagDirectory followed by findPeaks command from HOMER version 4.9.1 (Heinz et al., 2010) to identify peaks of ChIP-seq enrichment over background. A false discovery rate (FDR) threshold of 0.001 was used for all data sets. Regions that overlap with blacklist identified by the ENCODE project were filtered out. The total number of mapped reads in each sample was normalized to ten million mapped reads. ChIP-seq data were visualized by preparing custom tracks for the UCSC Genome browser. For identifying enhancer regions that were differentially acetylated in at least one of four conditions (FDR < 0.05, > 2-fold changes in any pairwise comparison), we used the getDifferentialPeaksReplicates.pl with parameters -genome hg19 -balanced -t H3K27ac_L1/ H3K27ac_L2/ -b H3K27ac_R1/ H3K27ac_R2/ -p enhancers.bed from HOMER package and then merged using mergePeaks-size given. For the clustering of enhancers, we used GENE-E (Broad Institute) set to global comparison and average-centered. The value of K was chosen at 5 because lower values failed to identify all meaningful clusters and higher values subdivided existing clusters. The third enhancer cluster (C3) in Supplementary Fig. 2c was further classified into two clusters (e2 and e3) in Fig. 2a based on the changes in H3K27ac between IFN-γ-stimulated (G) and IFN-γ-primed LPS-stimulated (GL) macrophages. For the distribution plot of ChIP-seq signals in Fig. 4c and g, we used the annotatePeaks.pl command with parameters -size 2000 -hist 10 to generate histograms for the average distribution of normalized tag densities. For functional annotations of the enhancers, enriched GO Biological Process and MSigDB Pathways were compiled from the GREAT version 3.0.0 (McLean et al., 2010) on each subset of enhancer-associated genes. GO and MSigDB pathways were ranked based on *p*-values. Normalized tag counts used in plotting the boxplots for ChIP-seq and ATAC-seq data are available as Source Data in Excel format.

Motif enrichment analysis. de novo and known motif analysis were performed on ±100 bp centered on the ATAC-seq peak that overlapped either PU.1 or C/EBPβ, using command findMotifsGenome.pl from HOMER package. Peak sequences were compared to random genomic fragments of the same size and normalized G + C content to identify motifs enriched in the targeted sequences.

LNA transfection. LNAs (LNATM longRNA GapmeR) were designed and synthesized by Exiqon. Knockdown experiments with LNAs were performed using Human Monocyte Nucleofector buffer (Lonza Cologne) and the AMAXA Nucleofector System program Y001 for human monocytes according to the manufacturer's instructions. Two different LNATM longRNA GapmeRs (negative control A and B) were used as control. Cells were harvested for RNA analysis 24 h after transfection. The following LNAs were used for knockdown studies of *IL10* eRNAs. Custom LNA for *IL10* eRNA (HSS-16): ATAGAGAGGAGATGCA, GCAGTCTAGCTTGGTG. Custom LNA for *IL10* eRNA (HSS + 6): GGATTTCG CGGGAGTT, TCCTAGTGCCAGAAGC.

Statistical analysis. Statistical tests were selected based on appropriate assumptions with respect to data distribution and variance characteristics. Wilcoxon signed-rank test or two-tailed paired *t*-test was used for the statistical analysis of two paired samples. Welch's *t*-test or unpaired Student's *t*-test was used for the statistical analysis of two non-paired samples. Statistical significance was defined as *p* < 0.05. The whiskers of boxplots represent the 10–90th percentiles of the data. Statistical analyses were performed using GraphPad Prism 7.

Reporting summary. Further information on research design is available in the Nature Research Reporting Summary linked to this article.

Data availability

RNA-seq, ChIP-seq, and ATAC-seq data that support the findings of this study have been deposited in GenBank with the GSE120945 and GSE130567 accession codes.

Received: 26 September 2018 Accepted: 25 June 2019

Published online: 25 July 2019

References

- Ginhoux, F., Schultze, J. L., Murray, P. J., Ochando, J. & Biswas, S. K. New insights into the multidimensional concept of macrophage ontogeny, activation and function. *Nat. Immunol.* **17**, 34–40 (2016).
- Amit, I., Winter, D. R. & Jung, S. The role of the local environment and epigenetics in shaping macrophage identity and their effect on tissue homeostasis. *Nat. Immunol.* **17**, 18–25 (2016).
- Monticelli, S. & Natoli, G. Transcriptional determination and functional specificity of myeloid cells: making sense of diversity. *Nat. Rev. Immunol.* **17**, 595 (2017).
- Lawrence, T. & Natoli, G. Transcriptional regulation of macrophage polarization: enabling diversity with identity. *Nat. Rev. Immunol.* **11**, 750–761 (2011).
- Murray, P. J. Macrophage activation and polarization: nomenclature and experimental guidelines. *Immunity* **41**, 14–20 (2014).
- Hu, X., Chen, J., Wang, L. & Ivashkiv, L. B. Crosstalk among Jak-STAT, Toll-like receptor, and ITAM-dependent pathways in macrophage activation. *J. Leukoc. Biol.* **82**, 237–243 (2007).
- Hu, X. & Ivashkiv, L. B. Cross-regulation of signaling pathways by interferon-γ: implications for immune responses and autoimmune diseases. *Immunity* **31**, 539–550 (2009).
- Qiao, Y. et al. Synergistic activation of inflammatory cytokine genes by interferon-γ-induced chromatin remodeling and toll-like receptor signaling. *Immunity* **39**, 454–469 (2013).
- Su, X. et al. Interferon-γ regulates cellular metabolism and mRNA translation to potentiate macrophage activation. *Nat. Immunol.* **16**, 838–849 (2015).
- Ivashkiv, L. B. IFNγ: signalling, epigenetics and roles in immunity, metabolism, disease and cancer immunotherapy. *Nat. Rev. Immunol.* **18**, 545–558 (2018).
- Toshchakov, V. et al. TLR4, but not TLR2, mediates IFN-β-induced STAT1α/β-dependent gene expression in macrophages. *Nat. Immunol.* **3**, 392 (2002).
- Murray, P. J. & Smale, S. T. Restraint of inflammatory signaling by interdependent strata of negative regulatory pathways. *Nat. Immunol.* **13**, 916 (2012).
- Saeed, S. et al. Epigenetic programming of monocyte-to-macrophage differentiation and trained innate immunity. *Science* **345**, 1251086 (2014). <https://doi.org/10.1126/science.1251086>.
- Netea, M. G. et al. Trained immunity: a program of innate immune memory in health and disease. *Science* **352**, aaf1098 (2016). <https://doi.org/10.1126/science.aaf1098>.
- Netea, M. G., Latz, E., Mills, K. H. G. & O'Neill, L. A. J. Innate immune memory: a paradigm shift in understanding host defense. *Nat. Immunol.* **16**, 675–679 (2015).
- Park, S. H. Type I interferons and the cytokine TNF cooperatively reprogram the macrophage epigenome to promote inflammatory activation. *Nat. Immunol.* **18**, 1104–1116 (2017).
- Lavin, Y. et al. Tissue-resident macrophage enhancer landscapes are shaped by the local microenvironment. *Cell* **159**, 1312–1326 (2014).
- Glass, C. K. & Natoli, G. Molecular control of activation and priming in macrophages. *Nat. Immunol.* **17**, 26–33 (2016).
- Kaikkonen, Minna U. et al. Remodeling of the enhancer landscape during macrophage activation is coupled to enhancer transcription. *Mol. Cell* **51**, 310–325 (2013).
- Ostuni, R. et al. Latent enhancers activated by stimulation in differentiated cells. *Cell* **152**, 157–171 (2013).

21. Ehrh, S. et al. Reprogramming of the macrophage transcriptome in response to interferon- γ and mycobacterium tuberculosis: signaling roles of nitric oxide synthase-2 and phagocyte oxidase. *J. Exp. Med.* **194**, 1123–1140 (2001).
22. Xue, J. et al. Transcriptome-based network analysis reveals a spectrum model of human macrophage activation. *Immunity* **40**, 274–288 (2014).
23. Bhatt, DevM. et al. Transcript dynamics of proinflammatory genes revealed by sequence analysis of subcellular RNA fractions. *Cell* **150**, 279–290 (2012).
24. Qiao, Y., Kang, K., Giannopoulou, E., Fang, C. & Ivashkiv, LionelB. IFN- γ induces histone 3 lysine 27 trimethylation in a small subset of promoters to stably silence gene expression in human macrophages. *Cell Rep.* **16**, 3121–3129 (2016).
25. Kang, K. et al. Interferon- γ represses M2 gene expression in human macrophages by disassembling enhancers bound by the transcription factor MAF. *Immunity* **47**, 235–250.e234 (2017).
26. Piccolo, V. et al. Opposing macrophage polarization programs show extensive epigenomic and transcriptional cross-talk. *Nat. Immunol.* **18**, 530–540 (2017).
27. Czimmerer, Z. The transcription factor STAT6 mediates direct repression of inflammatory enhancers and limits activation of alternatively polarized macrophages. *Immunity* **48**, 75–90 (2018).
28. Teles, R. M. B. et al. Type I interferon suppresses type II interferon-triggered human anti-mycobacterial responses. *Science* **339**, 1448–1453 (2013).
29. Ho, H. H., Antoniv, T. T., Ji, J.-D. & Ivashkiv, L. B. Lipopolysaccharide-induced expression of matrix metalloproteinases in human monocytes is suppressed by IFN- γ via superinduction of ATF-3 and suppression of AP-1. *J. Immunol.* **181**, 5089–5097 (2008).
30. Hu, X. et al. IFN- γ suppresses IL-10 production and synergizes with TLR2 by regulating GSK3 and CREB/AP-1 proteins. *Immunity* **24**, 563–574 (2006).
31. Ivashkiv, L. B. & Donlin, L. T. Regulation of type I interferon responses. *Nat. Rev. Immunol.* **14**, 36–49 (2014).
32. Vahedi, G. et al. STATs Shape the active enhancer landscape of T cell populations. *Cell* **151**, 981–993 (2012).
33. Wienerroither, S. et al. Cooperative transcriptional activation of antimicrobial genes by STAT and NF- κ B pathways by concerted recruitment of the mediator complex. *Cell Rep.* **12**, 300–312 (2015).
34. Bancerek, J. et al. CDK8 kinase phosphorylates transcription factor STAT1 to selectively regulate the interferon response. *Immunity* **38**, 250–262 (2013).
35. Kagey, M. H. et al. Mediator and cohesin connect gene expression and chromatin architecture. *Nature* **467**, 430–435 (2010).
36. Allen, B. L. & Taatjes, D. J. The Mediator complex: a central integrator of transcription. *Nat. Rev. Mol. Cell Biol.* **16**, 155–166 (2015).
37. Cuartero, S. et al. Control of inducible gene expression links cohesin to hematopoietic progenitor self-renewal and differentiation. *Nat. Immunol.* **19**, 932–941 (2018).
38. Lam, M. T., Li, W., Rosenfeld, M. G. & Glass, C. K. Enhancer RNAs and regulated transcriptional programs. *Trends Biochem. Sci.* **39**, 170–182 (2014).
39. Bose, D. A. et al. RNA Binding to CBP Stimulates Histone Acetylation and Transcription. *Cell* **168**, 135–149.e122 (2017).
40. Sigova, A. A. et al. Transcription factor trapping by RNA in gene regulatory elements. *Science* **350**, 978–981 (2015).
41. Li, W., Notani, D. & Rosenfeld, M. G. Enhancers as non-coding RNA transcription units: recent insights and future perspectives. *Nat. Rev. Genet.* **17**, 207–223 (2016).
42. Chiche, L. Modular transcriptional repertoire analyses of adults with systemic lupus erythematosus reveal distinct type I and type II interferon signatures. *Arthritis Rheumatol.* **66**, 1583–1595 (2014).
43. Hall, J. C. Precise probes of type II interferon activity define the origin of interferon signatures in target tissues in rheumatic diseases. *Proc. Natl Acad. Sci. USA* **109**, 17609–17614 (2012).
44. Glass, C. K. & Saijo, K. Nuclear receptor transrepression pathways that regulate inflammation in macrophages and T cells. *Nat. Rev. Immunol.* **10**, 365–376 (2010).
45. Hutchins, A. P., Poulain, S. & Miranda-Saavedra, D. Genome-wide analysis of STAT3 binding in vivo predicts effectors of the anti-inflammatory response in macrophages. *Blood* **119**, e110–e119 (2012).
46. Ip, W. K. E., Hoshi, N., Shouval, D. S., Snapper, S. & Medzhitov, R. Anti-inflammatory effect of IL-10 mediated by metabolic reprogramming of macrophages. *Science* **356**, 513–519 (2017).
47. Pattison, M. J., MacKenzie, K. F. & Arthur, J. S. C. Inhibition of JAKs in macrophages increases lipopolysaccharide-induced cytokine production by blocking IL-10-mediated feedback. *J. Immunol.* **189**, 2784–2792 (2012).
48. Hu, X. IFN- γ suppresses IL-10 production and synergizes with TLR2 by regulating GSK3 and CREB/AP-1 proteins. *Immunity* **24**, 563–574 (2006).
49. O’Neill, L. A. J., Kishton, R. J. & Rathmell, J. A guide to immunometabolism for immunologists. *Nat. Rev. Immunol.* **16**, 553 (2016).
50. Van den Bossche, J., O’Neill, L. A. & Menon, D. Macrophage immunometabolism: where are we (going)? *Trends Immunol.* **38**, 395–406 (2017).
51. Phan, A. T., Goldrath, A. W. & Glass, C. K. Metabolic and epigenetic coordination of T cell and macrophage immunity. *Immunity* **46**, 714–729 (2017).
52. Dobin, A. et al. STAR: ultrafast universal RNA-seq aligner. *Bioinformatics* **29**, 15–21 (2013).
53. Trapnell, C. et al. Transcript assembly and quantification by RNA-Seq reveals unannotated transcripts and isoform switching during cell differentiation. *Nat. Biotech.* **28**, 511–515 (2010).
54. Robinson, M. D., McCarthy, D. J. & Smyth, G. K. edgeR: a Bioconductor package for differential expression analysis of digital gene expression data. *Bioinformatics* **26**, 139–140 (2010).
55. McCarthy, D. J., Chen, Y. & Smyth, G. K. Differential expression analysis of multifactor RNA-Seq experiments with respect to biological variation. *Nucleic Acids Res.* **40**, 4288–4297 (2012).
56. Liao, Y., Smyth, G. K. & Shi, W. featureCounts: an efficient general purpose program for assigning sequence reads to genomic features. *Bioinformatics* **30**, 923–930 (2014).
57. Huang, D. W., Sherman, B. T. & Lempicki, R. A. Systematic and integrative analysis of large gene lists using DAVID bioinformatics resources. *Nat. Protoc.* **4**, 44–57 (2008).
58. Buenrostro, J. D., Giresi, P. G., Zaba, L. C., Chang, H. Y. & Greenleaf, W. J. Transposition of native chromatin for fast and sensitive epigenomic profiling of open chromatin, DNA-binding proteins and nucleosome position. *Nat. Meth.* **10**, 1213–1218 (2013).

Acknowledgements

The work at Hospital for Special Surgery was supported by grants from the NIH (to LBI). Work at Chungbuk National University was performed by Kyuho K. and was supported by National Research Foundation of Korea grant funded by the Korean government (No. NRF-2019R1F1A1A1063848).

Author contributions

Kyuho K. and M.B. performed experiments and bioinformatic analysis and wrote the manuscript. S.P. and Keunsoo K. performed bioinformatic analysis. S.B. and K.-H. P.-M. performed Seahorse experiments. L.B.I. conceptualized and oversaw the project and edited the manuscript.

Additional information

Supplementary Information accompanies this paper at <https://doi.org/10.1038/s41467-019-11147-3>.

Competing interests: The authors declare no competing interests.

Reprints and permission information is available online at <http://npg.nature.com/reprintsandpermissions/>

Peer review information: *Nature Communications* thanks W. K. Eddie Ip and other anonymous reviewer(s) for their contribution to the peer review of this work.

Publisher’s note: Springer Nature remains neutral with regard to jurisdictional claims in published maps and institutional affiliations.



Open Access This article is licensed under a Creative Commons Attribution 4.0 International License, which permits use, sharing, adaptation, distribution and reproduction in any medium or format, as long as you give appropriate credit to the original author(s) and the source, provide a link to the Creative Commons license, and indicate if changes were made. The images or other third party material in this article are included in the article’s Creative Commons license, unless indicated otherwise in a credit line to the material. If material is not included in the article’s Creative Commons license and your intended use is not permitted by statutory regulation or exceeds the permitted use, you will need to obtain permission directly from the copyright holder. To view a copy of this license, visit <http://creativecommons.org/licenses/by/4.0/>.

© The Author(s) 2019